ELSEVIER

Journal of Fluids and Structures 24 (2008) 418–435

JOURNAL OF FLUIDS AND STRUCTURES

www.elsevier.com/locate/jfs

Reservoir water level effects on nonlinear dynamic response of arch dams

M. Akkose*, A. Bayraktar, A.A. Dumanoglu

Department of Civil Engineering, Karadeniz Technical University, 61080 Trabzon, Turkey

Received 18 November 2005; accepted 5 August 2007
Available online 26 November 2007

Abstract

In this study, reservoir water level effects on nonlinear dynamic response of arch dams are investigated. For this purpose, the nonlinear behaviour of the dam concrete is idealized as elasto-plastic using the Drucker–Prager model based on the associated flow rule assumption. Water in the reservoir is represented by the Lagrangian (displacement-based) fluid finite elements. The program NONSAP is modified for elasto-plastic analysis of fluid–structure systems and employed in the response calculations. Nonlinear dynamic analysis of an arch dam subjected to earthquake ground motion is performed for five different water levels. The El-Centro N–S component of the Imperial Valley earthquake, on May 18, 1940, has been used as the ground motion. The crest displacements, the maximum tensile stresses on the upstream and downstream faces of the dam and the time history of the yield function of an element in the dam body are presented. The results obtained from nonlinear analyses for different water levels are compared with each other. It is apparent that the reservoir water level effects must be considered in the elasto-plastic analyses of arch dams to earthquake ground motion.

Keywords: Arch dams; Dam–water–foundation rock interaction; Reservoir water level effect; Lagrangian approach; Nonlinear dynamic analysis; Drucker–Prager model; Earthquake ground motion

1. Introduction

The prediction of the actual dynamic response of an arch dam to earthquake loadings is a very complicated problem and depends on several factors such as interaction of the dam with its foundation rock and water in reservoir, computer modelling and selected material properties, etc. Therefore, an efficient method is required to properly assess the safety of an arch dam located in regions with significant seismicity. From this point of view, nonlinear dynamic analysis of arch dams for earthquake ground motions should be based on a detailed analytical model. Furthermore, this model should be capable of representing correctly both the materially nonlinear behaviour and the three-dimensional nature of the dam–water–foundation system that account for the interaction effects of the foundation rock and the impounded water.

Interaction between the dam and impounded water is an important factor affecting the dynamic response of arch dams during earthquake ground motion. When an arch dam–water system is subjected to a dynamic effect such as earthquake, hydrodynamic pressures in excess of hydrostatic pressures occur on the dam due to the vibration of the

*Corresponding author. Tel.: +90 4623772628; fax: +90 4623772606.
E-mail address: akkose@ktu.edu.tr (M. Akkose).

0889-9746/$ - see front matter
doi:10.1016/j.jfluidstructs.2007.08.007

Nomenclature

$\mathbf{B}$	strain–displacement matrix
c	cohesion
C_{11}	bulk modulus of fluid
C_{22}, C_{33}, C_{44}	constraint parameters for fluid
$\mathbf{C}_c$	damping matrix of coupled system
$d\lambda$	proportionality factor
$\mathbf{D}_e^n$	elastic constitutive matrix (ECM)
$\mathbf{D}_{ep}^n$	elasto-plastic constitutive matrix (EPCM)
f	yield function
G	shear modulus
$\mathbf{I}_1$	first invariant of stress tensor
$\mathbf{J}_2$	second invariant of deviatoric stress tensor
k	a constant which depends on cohesion c and angle of internal friction ϕ
K	bulk modulus
$\mathbf{K}_f$	stiffness matrix of fluid system
$\mathbf{K}_f^*$	system stiffness matrix including the free surface stiffness of fluid system
$\mathbf{K}_c$	stiffness matrix of coupled system
$\mathbf{M}_f$	mass matrix of fluid system
$\mathbf{M}c$	mass matrix of coupled system
P	pressures which are equal to mean stresses
P_x, P_y, P_z	rotational stresses of fluid
r	scaling factor
$\mathbf{R}$	load vector
$\mathbf{R}_f$	time-varying nodal force vector of fluid system
$\mathbf{R}_c$	external load vector of coupled system
s_{ij}	deviatoric stress tensor
$\mathbf{S}_f$	stiffness matrix of free surface of fluid system
T	kinetic energy of fluid system
$\mathbf{U}$	nodal displacements vector
$\mathbf{U}_f$	nodal displacement vector of fluid system
$\mathbf{U}_{sf}$	vertical nodal displacement vector of fluid system
$\mathbf{U}_c$	displacement vector of coupled system
$\dot{\mathbf{U}}_f$	nodal velocity vector of fluid system
$\dot{\mathbf{U}}_c$	velocity vector of coupled system
$\ddot{\mathbf{U}}_f$	nodal acceleration vector of fluid system
$\ddot{\mathbf{U}}_c$	acceleration vector of coupled system
w_x, w_y and w_z	rotations about the cartesian axis x, y and z
α	a constant which depends on cohesion c and angle of internal friction ϕ
δ_{ij}	Kronecker delta
ε_{ij}^n	strains at the end of nth loading increment
$\varepsilon_{ij}^{n+1/2}$	strains at $(n+1/2)$th loading increment
ε_{ij}^{n+1}	strains at $(n+1)$th loading increment
ε_v	volumetric strain of fluid,
π_e	total strain energy of fluid system
π_s	free surface potential energy of fluid system
σ_{ij}^n	stresses at the end of nth loading increment
$\sigma_{ij}^{n+1/2}$	stresses at $(n+1/2)$th loading increment
σ_{ij}^{n+1}	stresses at $(n+1)$th loading increment
ϕ	angle of internal friction

dam and water in the reservoir. These hydrodynamic pressures and the deformation of the dam interact with each other (Perumalswami and Kar, 1973). Therefore, the water level effect on the earthquake response of arch dams must be considered in the dynamic analysis. The magnitude of the hydrodynamic effects on an arch dam during earthquakes is based on the variation of water level in the reservoir. The reservoir water level varies according to season and can considerably affect the response of arch dams during earthquakes. The importance of the hydrodynamic effects on the behaviour of arch dams subjected to earthquake ground motions has long been recognized (Perumalswami and Kar, 1973; Fok and Chopra, 1986a, b; Tan and Chopra, 1995a, b). In the previous studies, the complex frequency functions have been used to define dam–water interactions and the concrete material was assumed to be linearly elastic. They have shown that the hydrodynamic pressures play an important role on the dynamic response of arch dams. In these studies, the reservoir was generally considered as empty or full. Proulx et al. (2001) have experimentally and numerically investigated the variation of the resonant frequencies of the Emosson arch dam for four different water levels.

On the other hand, equilibrium equations for the system and kinematic relations for the compatibility between strain and displacements should be verified for any nonlinear stress analysis problems. In addition, constitutive relations for the stress and strain behaviour of the material should be determined. The great error in currently available techniques for the nonlinear finite element analysis lies in the selection of an appropriate material model. Once the material model is selected, the stress state can be evaluated for a given strain state. The strain state is estimated from the incremental equilibrium equations of the system and subsequently from the kinematic relations (Chen and Mizuno, 1990). Concrete, capable of displaying nonlinear characteristics, is an essential material in many structures such as arch dams. There are several approaches to model the complicated stress–strain behaviour of concrete. In this regard, the theories based on plasticity and fracture mechanics are commonly applied in most of the engineering analysis. However, only a few studies taking into account material nonlinearity have been performed to investigate the dynamic behaviour of concrete arch dams. Kuo (1982) suggested an interface smeared crack approach to model the contraction joints and applied this technique to dynamic analysis of arch dams. Hall (1998) used a simple smeared crack model for modelling the contraction and construction joints. Valliappan et al. (1999) utilized a continuum damage mechanics approach to

investigate seismic response of arch dams. Espandar and Lotfi (2003) compared nonorthogonal smeared crack and an elasto-plastic model based on Mohr–Coulomb yield criterion for dynamic analysis of concrete arch dams. Akkose (2004) also used an elasto-plastic model based on the Drucker–Prager yield criterion in the nonlinear dynamic analysis of arch dams. In the continuum models, such as elasto-plastic models and smeared crack models, the dam body is assumed as a monolith and the nonlinear behaviour of the mass concrete of the dam body is investigated.

In this study, water level effects on the nonlinear dynamic response of an arch dam including dam–water–foundation interaction is investigated by a Lagrangian approach in which a step-by-step integration technique is employed. The stress–strain behaviour of the dam concrete is idealized using a three-dimensional Drucker–Prager model based on the associated flow rule assumption. To this end, the three-dimensional version of Drucker–Prager model is incorporated into a general finite element computer program NONSAP (Bathe et al., 1974) using mid-point integration method, which is suitable for general structural analysis programs. In addition, the eight-noded three-dimensional version of the Lagrangian fluid finite element put forward by Wilson and Khalvati (1983) is coded by authors in the FORTRAN language and incorporated into the NONSAP program. The modified version of the NONSAP program for elasto-plastic analysis of fluid–structure systems was employed in the response calculations. Nonlinear dynamic analyses of an arch dam on both rigid and flexible foundation rock were performed for five different water levels. The results obtained from nonlinear analyses for different water levels are compared with each other.

2. The Drucker—Prager model

There are many criteria for the determination of the yield surface or yield function of materials. The Drucker–Prager criterion is widely used for frictional materials such as rock and concrete. Drucker and Prager (1952) obtained a convenient yield function to determine elasto-plastic behaviour of concrete, smoothing the Mohr–Coulomb criterion. This function is defined as

$$f = \alpha \mathrm{I}_1 + \sqrt{\mathrm{J}_2} - k, \tag{1}$$

where I_1 is the first invariant of stress tensor σ_{ij} and J_2 is the second invariant of deviatoric stress tensor s_{ij}; α and k are constants which depend on cohesion c and angle of internal friction ϕ of the material given by

$$\alpha = \frac{2\sin\phi}{\sqrt{3}(3-\sin\phi)}, \quad k = \frac{6c\cos\phi}{\sqrt{3}(3-\sin\phi)}. \tag{2, 3}$$

The implementation of the Drucker–Prager model to the general nonlinear finite element computer program NONSAP is described herein. More details of the implementation of the model can be found in Chen and Mizuno (1990). The three-dimensional version of the model based on the associated flow rule assumption is incorporated into the NONSAP program using a mid-point integration method based on the two-stepped Runge–Kutta method. In this method, the first step is called the mid-increment step, and the second step is called the full-increment step. The mid-point integration method reduces the computational time and provides the necessary accuracy of the solution within the small strain increment.

2.1. Mid-increment step

It is assumed that stresses and strains in an element are σ_{ij}^n and ε_{ij}^n at the end of the nth loading increment, respectively. According to the stress state (elastic or plastic) in the element, either the elastic constitutive matrix (ECM) $\mathbf{D}_e$ or the elasto-plastic constitutive matrix (EPCM) $\mathbf{D}_{ep}$ is used to calculate the current element tangent stiffness.

Applying first the half of the incremental loads to the discretized system stiffness $\mathbf{K}^n$, incremental strains $\mathrm{d}\varepsilon_{ij}^{n+1/2}$ at the $(n+1/2)$th increment are estimated from the kinematic condition as follows:

$$\mathrm{d}\mathbf{U}^{n+1/2} = (\mathbf{K}^n)^{-1}\left(\frac{1}{2}\,\mathrm{d}\mathbf{R}\right) \quad \text{in structural level,} \tag{4}$$

$$\mathrm{d}\varepsilon^{n+1/2} = \mathbf{B}\,\mathrm{d}\mathbf{U}^{n+1/2} \quad \text{in an element level,} \tag{5}$$

where $\mathbf{U}$, $\mathbf{R}$ and $\mathbf{B}$ are nodal displacements vector, load vector and strain-displacement matrix, respectively. Subsequently, the corresponding stress increments $\mathrm{d}\sigma_{ij}^{n+1/2}$ in all elements are estimated by using the current constitutive matrix $\mathbf{D}_e$ or $\mathbf{D}_{ep}$. Then, the stresses $\sigma_{ij}^{n+1/2}$ for all elements at the end of the $(n+1/2)$th loading increment are approximated from the stresses σ_{ij}^n:

$$\mathrm{d}\sigma_{ij}^{n+1/2} = \mathbf{D}_e\,\mathrm{d}\varepsilon_{ij}^{n+1/2} \quad \text{or} \quad \mathrm{d}\sigma_{ij}^{n+1/2} = \mathbf{D}_{ep}^n\mathrm{d}\varepsilon_{ij}^{n+1/2}, \quad \sigma_{ij}^{n+1/2} = \sigma_{ij}^n + \mathrm{d}\sigma_{ij}^{n+1/2}. \tag{6, 7}$$

The main purpose of the calculation made at the mid-increment step is to correct the stresses $\sigma_{ij}^{n+1/2}$ in all elements if necessary and to construct for each element a new constitutive matrix. In the following, the calculation steps at mid-increment are presented.

Step 1: Preliminary calculation. The first invariant $\mathrm{I}_1^{n+1/2}$ of stress tensor and second invariant $\mathrm{J}_2^{n+1/2}$ of deviatoric stress tensor are computed by using the stresses $\sigma_{ij}^{n+1/2}$.

Step 2: Check for tension cracking. When the stress state exceeds the apex of the yield surface, it will shift the hydrostatic stress component to the corresponding hydrostatic pressure at the apex (Fig. 1) as follows:

$$\tilde{\sigma}_{ii}^{n+1/2} = \sigma_{ii}^{n+1/2} - \frac{1}{3}\left(I_1^{n+1/2} - \frac{k}{\alpha}\right). \tag{8}$$

Thus, the adjusted normal stresses can be estimated from Eq. (8), while the shearing stresses $\sigma_{12}^{n+1/2}, \sigma_{23}^{n+1/2}$, and $\sigma_{31}^{n+1/2}$ remain unchanged. Subsequently, the following steps should be performed.

Step 3: Check for a previously plastic element. If the element is in the plastic state at the end of the nth increment, the element must be checked to determine whether it has undergone the plastic loading by calculating the proportionality factor $\mathrm{d}\lambda$ given by

$$\mathrm{d}\lambda^{n+1/2} = \frac{1}{H}\left[3K\alpha\,\mathrm{d}\varepsilon_v^{n+1/2} + G\frac{1}{\sqrt{J_2^n}}s_{kl}^n\,\mathrm{d}e_{kl}^{n+1/2}\right], \tag{9}$$

where s_{kl}^n are the deviatoric stresses at the end of the nth load increment and $\mathrm{d}e_{kl}^{n+1/2}$ are the deviatoric strain increments at the end of the $(n+1/2)$th load increment; $\mathrm{d}\varepsilon_v^{n+1/2}$ is the sum of strain increments at the end of the $(n+1/2)$th load increment. In Eq. (9), H is given by

$$H = 9K\alpha^2 + G, \tag{10}$$

where K and G are the bulk and shear modulus of the material, respectively. If $\mathrm{d}\lambda^{n+1/2}$ has a negative value, the element has undergone a plastic unloading. Then, the ECM is assigned to compute the subsequent tangent stiffness of the system as follows:

$$\mathbf{D}_e = \begin{bmatrix} K+(4/3)G & K-(2/3)G & K-(2/3)G & 0 & 0 & 0 \\ K-(2/3)G & K+(4/3)G & K-(2/3)G & 0 & 0 & 0 \\ K-(2/3)G & K-(2/3)G & K+(4/3)G & 0 & 0 & 0 \\ 0 & 0 & 0 & G & 0 & 0 \\ 0 & 0 & 0 & 0 & G & 0 \\ 0 & 0 & 0 & 0 & 0 & G \end{bmatrix}. \tag{11}$$

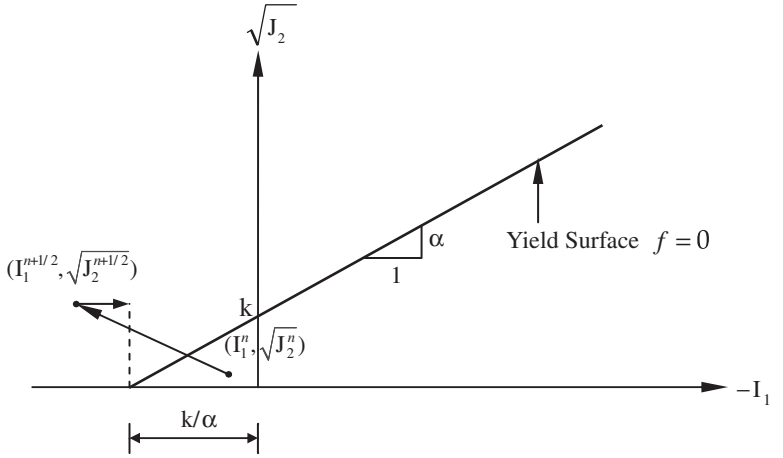

Fig. 1. Check for tensile stress (Chen and Mizuno, 1990).

On the other hand, if $d\lambda^{n+1/2}$ has a positive value, the element is assumed to remain plastic during the $(n+1)$th loading increment. Then, the stress state $\sigma_{ij}^{n+1/2}$ is scaled back to the failure or yield surface. In the scaling back procedure, the hydrostatic component I_1 and the principal directions of the stress tensor remain unchanged, while the deviatoric stress components are reduced proportionality by the scaling factor r_1. The scaling factor is expressed by

$$r_1 = \Delta T / \sqrt{J_2^{n+1/2}}, \tag{12}$$

where ΔT is the positive value defined by

$$\Delta T = -\alpha I_1^{n+1/2} + k. \tag{13}$$

Thus, the scaled-back stresses are given by

$$\tilde{\sigma}_{ij}^{n+1/2} = r_1 s_{ij}^{n+1/2} + \delta_{ij} \tfrac{1}{3} I_1^{n+1/2}, \tag{14}$$

where $I_1^{n+1/2} = \sigma_{11}^{n+1/2} + \sigma_{22}^{n+1/2} + \sigma_{33}^{n+1/2}$ and δ_{ij} is the Kronecker delta, its value is 1 for $i = j$, 0 for $i \neq j$.

Utilizing the above stress components, the EPCM can be computed for the construction of a new tangent stiffness matrix at the mid-increment as

$$\mathbf{D}_{ep}^{n+1/2} = \mathbf{D}_e - \mathbf{D}_p^{n+1/2}, \tag{15}$$

where $\mathbf{D}_e$ is the ECM given previously in Eq. (11) and $\mathbf{D}_p^{n+1/2}$ can be written as

$$\mathbf{D}_p^{n+1/2} = \frac{1}{H} \begin{bmatrix} H_{11}^2 & H_{11}H_{22} & H_{11}H_{33} & H_{11}H_{12} & H_{11}H_{13} & H_{11}H_{23} \\ H_{22}H_{11} & H_{22}^2 & H_{22}H_{33} & H_{22}H_{12} & H_{22}H_{13} & H_{22}H_{23} \\ H_{33}H_{11} & H_{33}H_{22} & H_{33}^2 & H_{33}H_{12} & H_{33}H_{13} & H_{33}H_{23} \\ H_{12}H_{11} & H_{12}H_{22} & H_{12}H_{33} & H_{12}^2 & H_{12}H_{13} & H_{12}H_{23} \\ H_{13}H_{11} & H_{13}H_{22} & H_{13}H_{33} & H_{13}H_{12} & H_{13}^2 & H_{13}H_{23} \\ H_{23}H_{11} & H_{23}H_{22} & H_{23}H_{33} & H_{23}H_{12} & H_{23}H_{13} & H_{23}^2 \end{bmatrix}, \tag{16}$$

in which the form of H is already given in Eq. (10). The components of this matrix are expressed as follows:

$$H_{ij} = 3K\alpha\delta_{ij} + \frac{G}{\sqrt{\tilde{J}_2^{n+1/2}}} \tilde{s}_{ij}^{n+1/2}, \tag{17}$$

where $\tilde{s}_{ij}^{n+1/2}$ are the scaled-back deviatoric stresses, and $\sqrt{\tilde{J}_2^{n+1/2}}$ can be computed from the scaled-back stresses $\tilde{\sigma}_{ij}^{n+1/2}$.

Step 4: Check for a previously elastic element. For the element that is previously in an elastic state at the end of the nth increment, the value of $f(= \alpha I_1 + \sqrt{J_2} - k)$ is given by

$$f^n = \alpha I_1^n + \sqrt{J_2^n} - k < 0, \tag{18}$$

where I_1^n and J_2^n are the first and second invariants of the stress tensor and deviatoric stress tensor obtained at the nth load increment. The value of f at the mid-increment can be evaluated via

$$f^{n+1/2} = \alpha I_1^{n+1/2} + \sqrt{J_2^{n+1/2}} - k. \tag{19}$$

To predict the value of f at the end of the $(n+1)$th increment, the following relationship is assumed:

$$f^{n+1} = f^n + 2(f^{n+1/2} - f^n). \tag{20}$$

If the estimated value f^{n+1} is still negative, it is assumed that the element remains in the elastic range during the $(n+1)$th increment. Thus, an ECM is assigned for this element during the $(n+1)$th incremental calculation. On the other hand, if f^{n+1} has a positive value, it is assumed that the element yields during this increment. In this case, a weighted average of the elastic and elasto-plastic constitutive matrices is employed. To construct the averaged matrix, the stress state $\sigma_{ij}^{n+1/2}$ at the mid-increment is scaled back to the yield surface by the scaled-back procedure defined previously. The averaged constitutive matrix is computed as

$$\mathbf{D}_{av}^{n+1/2} = r_2 \mathbf{D}_e + (1 - r_2)\mathbf{D}_{ep}^{n+1/2}, \tag{21}$$

where r_2 is the scaling factor and $\mathbf{D}_{ep}^{n+1/2}$ is the EPCM based on the scaled-back stresses. Here, the scaling factor may be computed by

$$r_2 = -f^n/[2(f^{n+1/2} - f^n)]. \tag{22}$$

2.2. Full-increment step

With the aid of the system tangent stiffness $\mathbf{K}^{n+1/2}$ after the $(n+1/2)$th increment, the $(n+1)$th incremental calculation is performed to obtain the displacement increment $\mathrm{d}\mathbf{U}^{n+1}$ by applying the full load increment $\mathrm{d}\mathbf{R}$. Subsequently, the strain increment $\mathrm{d}\varepsilon_{ij}^{n+1}$ for the element can be evaluated from the kinematic condition

$$\mathrm{d}\mathbf{U}^{n+1} = (\mathbf{K}^{n+1/2})^{-1}\,\mathrm{d}\mathbf{R} \quad \text{in structural level,} \tag{23}$$

$$\mathrm{d}\varepsilon^{n+1} = \mathbf{B}\mathrm{d}\mathbf{U}^{n+1} \quad \text{in an element level.} \tag{24}$$

The stress increment $\mathrm{d}\sigma_{ij}^{n+1}$ can be obtained by using the current constitutive matrix $\mathbf{D}_e$ or $\mathbf{D}_{ep}$, and finally the stresses σ_{ij}^{n+1} can be estimated by adding the stress increment $\mathrm{d}\sigma_{ij}^{n+1}$ to the stress σ_{ij}^n at the end of the nth loading increment,

$$\mathrm{d}\sigma_{ij}^{n+1} = \mathbf{D}_e\,\mathrm{d}\varepsilon_{ij}^{n+1} \text{ or } \mathrm{d}\sigma_{ij}^{n+1} = \mathbf{D}_{ep}^{n+1/2}\,\mathrm{d}\varepsilon_{ij}^{n+1}, \quad \sigma_{ij}^{n+1} = \sigma_{ij}^n + \mathrm{d}\sigma_{ij}^{n+1}. \tag{25, 26}$$

Procedures at the full-increment step are generally similar to those at mid-increment step. Therefore, only a brief description is given in the following.

Step 1*: Preliminary calculation.* The first invaryant I_1^{n+1} of stress tensor and the second invariant J_2^{n+1} of deviatoric stress tensor are computed by using the stresses σ_{ij}^{n+1}.

Step 2*: Check for tension cracking.* If the hydrostatic stress exceeds the apex value of the yield surface, it need be shifted to the level of the apex. The calculation procedure is the same with Section 2.1. Subsequently, the following steps should be performed.

Step 3*: Check for a previously plastic element.* If the EPCM or an averaged matrix has been used to determine the mid-increment tangent stiffness, the stress state in the element at the end of the $(n+1)$th increment is assumed to be plastic regardless of whether the stress state lies inside or outside the failure or yield surface. The final stress state is then scaled back to the failure or yield surface and the EPCM is constructed for the next incremental calculation.

Step 4*: Check for a previously elastic element.* On the other hand, for the element that was elastic at the mid-increment step, the yield condition must be checked i.e. the stress state is checked against the failure or the current yield surface. If $f^{n+1} = \alpha \mathrm{I}_1^{n+1} + \sqrt{\mathrm{J}_2^{n+1}} - k > 0$ is satisfied, the stress state is scaled back to the failure or yield surface and the EPCM is assigned for the next increment. Otherwise, the stress state remains unchanged and the ECM is used for the next incremental calculation.

3. Equations of motion based on the Lagrangian approach

In the Lagrangian approach, the fluid is assumed to be linearly elastic, inviscid and irrotational. For a general three-dimensional fluid, stress–strain relationships can be written in matrix form as follows:

$$\begin{Bmatrix} P \\ P_x \\ P_y \\ P_z \end{Bmatrix} = \begin{bmatrix} C_{11} & 0 & 0 & 0 \\ 0 & C_{22} & 0 & 0 \\ 0 & 0 & C_{33} & 0 \\ 0 & 0 & 0 & C_{44} \end{bmatrix} \begin{Bmatrix} \varepsilon_v \\ w_x \\ w_y \\ w_z \end{Bmatrix}, \tag{27}$$

where P, C_{11} and ε_v are the pressures which are equal to mean stresses, the bulk modulus and the volumetric strains of the fluid, respectively. Since irrotationality of the fluid is considered like penalty methods (Zienkiewicz and Taylor,

1989; Bathe, 1996), rotations and constraint parameters can be included in the stress–strain equations of the fluid. In Eq. (27), P_x, P_y, P_z are the rotational stresses; C_{22}, C_{33}, C_{44} are the constraint parameters and w_x, w_y and w_z are the rotations about the cartesian axis x, y and z, respectively.

In this study, the equations of motion of the fluid system were obtained using energy principles. Using the finite element method, the total strain energy of the fluid system may be written as

$$\pi_e = \frac{1}{2}\mathbf{U}_f^{\mathrm{T}}\mathbf{K}_f\mathbf{U}_f, \tag{28}$$

where $\mathbf{U}_f$ and $\mathbf{K}_f$ are the nodal displacement vector and the stiffness matrix of the fluid system, respectively. An important behaviour of fluid systems is the ability to displace without a change in volume. For reservoir and storage tanks this movement is in the form of sloshing waves in which the displacement is in the vertical direction. Therefore, the effects of surface waves and sloshing behaviour of the fluid must be taken into account. It is possible to describe the behaviour of the free surface of the fluid in terms of the potential energy of the fluid. The potential energy of the systems due to the free surface motion can be written as

$$\pi_s = \frac{1}{2}\int_A \mathbf{U}_{sf}^{\mathrm{T}}\rho_f g\mathbf{U}_{sf}\,\mathrm{d}A, \tag{29}$$

where ρ_f, $\mathbf{U}_{sf}$ and g are mass density of the fluid, a vector of free surface vertical displacements and the acceleration due to gravity, respectively. Using the finite element method, free surface potential energy can be obtained as

$$\pi_s = \frac{1}{2}\mathbf{U}_{sf}^{\mathrm{T}}\mathbf{S}_f\mathbf{U}_{sf}, \tag{30}$$

where $\mathbf{S}_f$ is stiffness matrix of the free surface of the fluid system. Also, kinetic energy of the system can be written as

$$\mathbf{T} = \frac{1}{2}\dot{\mathbf{U}}_f^{\mathrm{T}}\mathbf{M}_f\dot{\mathbf{U}}_f, \tag{31}$$

where $\dot{\mathbf{U}}_f$ and $\mathbf{M}_f$ are the nodal velocity vector and the mass matrix of the fluid system, respectively. The equations of motion for a system can be derived directly from Lagrange's equations. These equations are a direct result of applying Hamilton's variational principle under the specific condition that the energy and work terms can be expressed in terms of the generalized coordinates and of their time derivatives and variations (Clough and Penzien, 1993). If Eqs. (28), (30) and (31) are substituted into Lagrange's equations, the following set of equations is obtained:

$$\mathbf{M}_f\ddot{\mathbf{U}}_f + \mathbf{K}_f^*\mathbf{U}_f = \mathbf{R}_f, \tag{32}$$

where $\mathbf{K}_f^*$ and $\dot{\mathbf{U}}_f$ are the system stiffness matrix including the free surface stiffness and the nodal acceleration vector for the fluid system, respectively. $\mathbf{R}_f$ is a time-varying nodal force vector defined as $-\mathbf{M}_f a_g$ when the earthquake ground acceleration is applied to the fluid system in which a_g is ground acceleration vector. In the formation of the fluid element matrices, reduced integration orders were utilized. For the eight-noded three-dimensional fluid element, reduced integration order is chosen as $1 \times 1 \times 1$ (Bathe, 1996).

The equations of motion of the fluid system, Eq. (32), have a similar form with those of the structure system. To obtain the coupled equations of the fluid–structure system, the determination of the interface condition is required. Since the fluid is assumed to be inviscid, only the displacement in the normal direction to the interface is continuous. Using the interface condition, the equations of motion of the coupled system subjected to ground motion including damping effects are given by

$$\mathbf{M}_c\ddot{\mathbf{U}}_c + \mathbf{C}_c\dot{\mathbf{U}}_c + \mathbf{K}_c\mathbf{U}_c = \mathbf{R}_c, \tag{33}$$

in which $\mathbf{M}_c$, $\mathbf{C}_c$ and $\mathbf{K}_c$ are the mass, damping and stiffness matrices for the coupled system. $\mathbf{U}_c$, $\dot{\mathbf{U}}_c$ and $\ddot{\mathbf{U}}_c$ are the vectors of the displacement, velocity and acceleration, respectively. $\mathbf{R}_c$ is the vector of external load of the coupled system.

4. Numerical application and discussion

The selected arch dam for this study is Type 5 as suggested in the symposium on arch dams ICE (1968). The dimensions of the arch dam are in unit as shown in Fig. 2. Its height is chosen as 120 m to obtain realistic results. The other dimensions of the dam are determined according to this size.

The finite element idealization prepared for dam–water–foundation rock system is presented in Fig. 3. A two-dimensional view of the finite element mesh at the vertical crown section is also given in this figure. The depth of

reservoir is 120 m in the finite element idealization prepared for dam–water–foundation rock system. The upstream and banks boundary conditions of reservoir should be nonreflective not to affect numerical results. In this study, instead of the nonreflective boundary condition, the reservoir length is selected as three times of the reservoir depth to consider the damping effect arising from the propagation of pressure waves in the upstream direction as in the references, Calayır and Dumanoğlu (1993) and Calayır et al. (1996). Besides, the nodes at the upstream and bank boundaries are allowed to move along interfaces.

The nonlinear behaviour of dam concrete is idealized as elasto-plastic using the Drucker–Prager model based on the associated flow rule assumption. The elasticity modulus, mass density and Poisson's ratio of the dam concrete are taken as $2.7579 \times 10^7\,\mathrm{kN/m^2}$, $2483\,\mathrm{kg/m^3}$ and 0.20, respectively. The cohesion c and the angle of internal friction ϕ for elasto-plastic behaviour of the concrete are $3.75 \times 10^3\,\mathrm{kN/m^2}$ and 35°, respectively. Eight-noded three-dimensional solid elements are used to represent the dam. The number of the elements in the dam is 128.

The foundation rock is assumed to be linearly elastic and represented by eight-noded three-dimensional solid elements up to a certain distance from the dam. To avoid reflection of the outgoing waves, these elements are assumed to be massless. The elasticity modulus and Poisson's ratio of the foundation rock are taken as $5.5158 \times 10^7\,\mathrm{kN/m^2}$ and 0.20, respectively. One hundred and sixty-four three-dimensional elements are used in the finite element mesh of the foundation rock.

The fluid is assumed to be linearly elastic, inviscid and irrotational. The bulk modulus and mass density of the fluid are taken as $0.207 \times 10^7\,\mathrm{kN/m^2}$ and $1000\,\mathrm{kg/m^3}$, respectively. The rotation constraint parameters of the fluid about each Cartesian axis are taken as 1000 times of the bulk modulus. The optimum value of the rotation constraint parameter changes with the properties of material and it can be a different value for various problems. The parameter should be as high as necessary to enforce the rotational constraint but small enough to avoid causing numerical ill-conditioning in the assembled stiffness matrix. This parameter is generally taken as 100 times of the bulk modulus in two-dimensional fluid–structure problems. But, it is taken as 1000 times of the bulk modulus in three-dimensional fluid–structure problems due to the mentioned reasons (Calayır and Dumanoğlu, 1993; Calayır, 1994; Hamdan, 1999). In addition, 512 eight-noded three-dimensional fluid elements are used to represent the water in the reservoir.

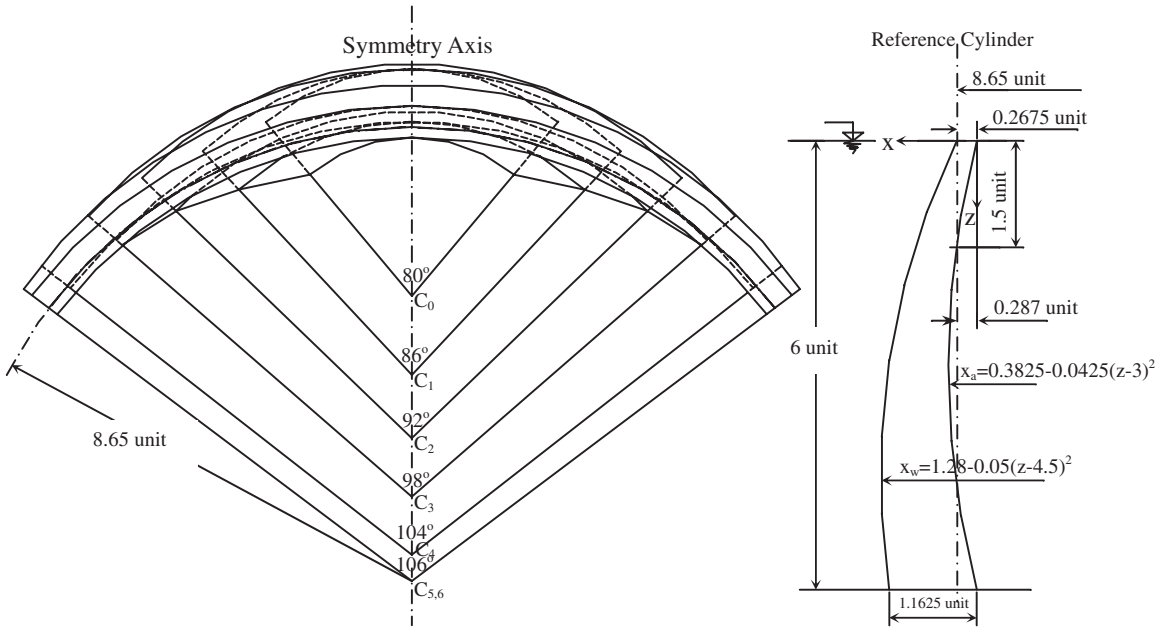

Level	C_0	C_1	C_2	C_3	C_4	C_5	C_6
Radius (unit)	3.67	5.29	6.64	7.72	8.54	8.80	8.50
Central Angle	80°	86°	92°	98°	104°	106°	106°

Fig. 2. The view in plan and vertical crown cross section of Type 5 arch dam (ICE, 1968).

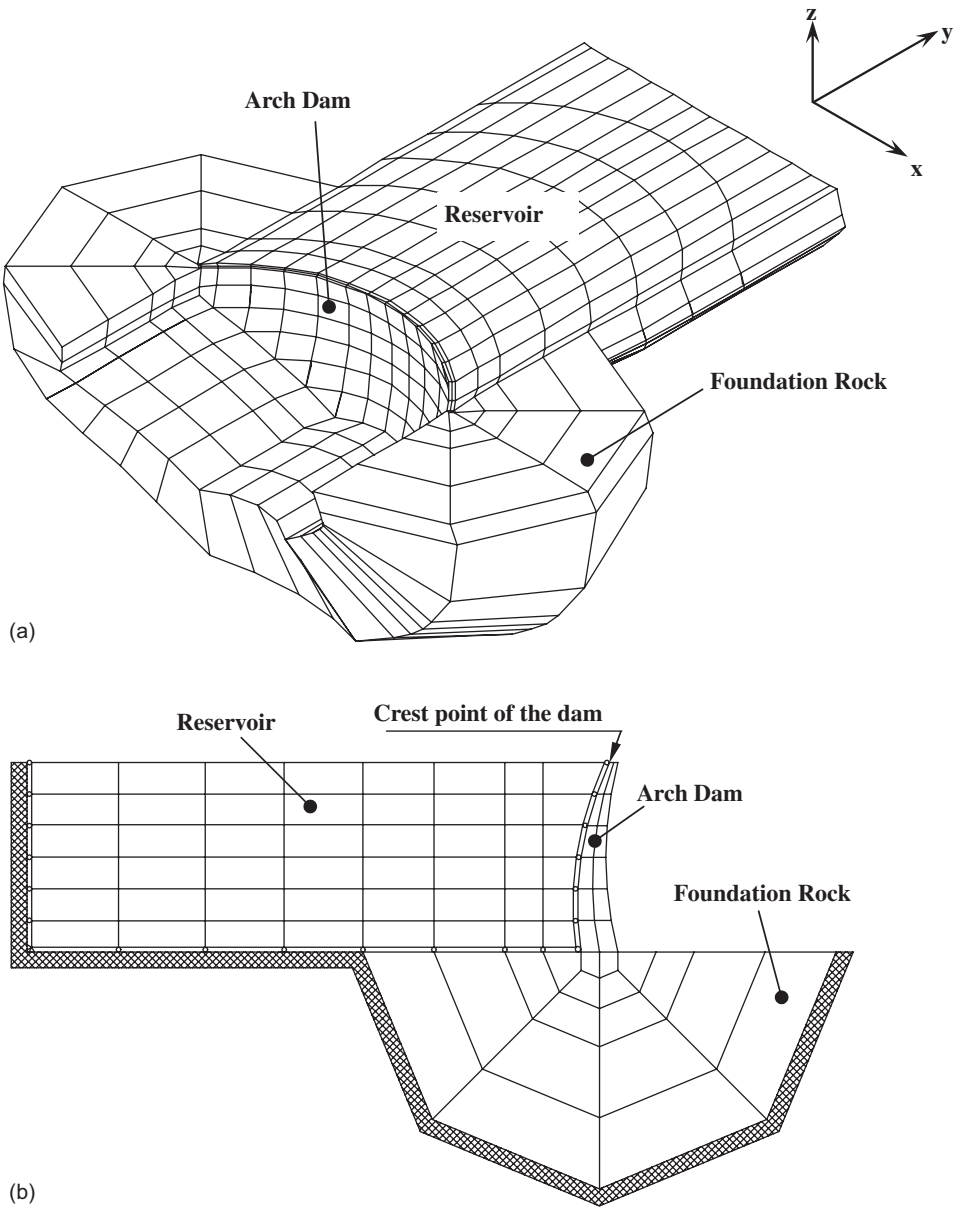

Fig. 3. The finite element mesh of dam–water–foundation rock interaction system of Type 5 arch dam: (a) axonometric view; (b) two-dimensional view at the vertical crown section.

The fluid is only able to transmit normal forces to both solid (canyon sides) and structure (dam) boundaries. This is because of its inviscid nature. The slip condition at the solid–fluid interface can be modelled by the use of constraint relations (Greeves, 1991; Calayır et al., 1996; Olson and Bathe, 1983; Zienkiewicz and Bettes, 1978), interface elements (Hamdan, 1999) or short and axially almost rigid link (truss) elements in the normal direction of the interface (Akkaş et al., 1979). At the interface of the reservoir–canyon, one node, which corresponds to the canyon side, of the link element is completely restrained (grounded), whereas the other is capable of moving in the translational directions. At the interface of the dam–reservoir, each of nodes of the link element allows translational motions. Thus, complete slip motion between fluid and the canyon and the fluid and the dam is still possible. The length and the elasticity modulus of the truss elements are taken as 0.001 m and $2 \times 10^{16}\,\mathrm{kN/m^2}$, respectively.

There are 1374 nodal points in the dam–water–foundation rock system (Fig. 3). At the boundaries of the dam–water–foundation rock system, there are 518 restrained degrees of freedom. Hence, the active degrees of freedom (or equations) for dam–water–foundation rock system are determined as 3604 in total.

The Wilson$-\theta$ method is used for the solution of the general equation of motion (Eq. (33)) of the coupled fluid–structure system in this study. This method requires that the damping matrix to be represented is in explicit form. This is accomplished using Rayleigh damping. The Rayleigh damping constants are taken to have the same values for both fluid and structure. The damping constants are calculated within a frequency range 2–15 Hz assuming 5% damping ratio. The first frequency of the system is 2.941 Hz. Accordingly, this frequency range ensures 5% damping ratio.

In this study, nonlinear dynamic analyses of the selected arch dam are performed according to the assumption that the dam is subjected to uniform ground motion along the dam–foundation interface. In other words, the same ground motion is used for all ground support points or the whole region of contact with the foundations is subjected to the same acceleration simultaneously. The El-Centro N–S record of Imperial Valley earthquake, on May 18, 1940, measured on a rock-like surface, is chosen as the ground motion (PEER: Pacific Earthquake Engineering Research Center, 2005). The record shown in Fig. 4 is applied to the coupled systems in the upstream–downstream direction (y-direction). In the analysis only the first 6.5 s of the earthquake is considered. The time step increment is chosen as 0.001 s for the integration. Hence, the number of time steps for solution of the coupled system is 6500.

Initial (static) stresses and displacements can have strong effects on the nonlinear dynamic response. Therefore, static analysis of the dam–water–foundation rock system under self-weight and the hydrostatic pressure is carried out to establish the initial condition for dynamic analysis. Subsequently, the linear and nonlinear dynamic analyses of the system are performed.

Water levels in the reservoir are considered as 40, 60, 80, 100 and 120 m to investigate the water level effects on the nonlinear dynamic response of the selected arch dam. The time-history of displacements at the dam crest for elasto-plastic analysis of the selected arch dam on rigid foundation rock is presented in Fig. 5, and that on flexible foundation rock is presented in Fig. 6. In these figures, nonlinear results are compared with linear results. In addition, the absolute maximum horizontal crest displacements of the dam on rigid and flexible foundation rock for linear and elasto-plastic analyses are presented in Table 1.

It is shown from Figs. 5and 6 and Table 1 that the crest displacements increase for the linear and elasto-plastic analyses of the dam on both rigid and flexible foundation rock as the water level in the reservoir increases. But, the crest displacements of the dam on flexible foundation rock are greater than those on a rigid one. Comparison of the results obtained from linear and elasto-plastic analyses of the arch dam shows a drift in the crest displacements. This drift for the arch dam on rigid foundation rock starts after the water level reaches 100 m. However, the drift in the case of flexible foundation rock starts after the water level 60 m. The major source of the drift response is the cumulative strain that occurs when the stress state exceeds the apex of the failure or yield surface (see Fig. 1) due to the tensile stresses. In addition to this, elasto-plastic analysis shows that the drift direction is affected by the bias of the stress state caused by the hydrostatic pressure. This drift response is the main characteristic of the time-history of displacements in the elasto-plastic analyses because of extensive tensile stresses on the dam body. In Figs. 5 and 6, if the results of the elasto-plastic model and linear model are compared each other, a drift in the crest displacements of the arch dam is observed in the upstream direction ($+y$-direction in Fig. 3). Plastic deformations in dams to earthquake ground motions may occur in the downstream or upstream direction. In our study, the plastic deformations occur in the upstream direction, as in Espandar and Lotfi (2003).

Variation of right bank to left bank of the maximum tensile stresses at the section E–E shown in Fig. 7 is investigated for linear analysis. The yield functions obtained at element A (Fig. 7) selected in the dam body are investigated for

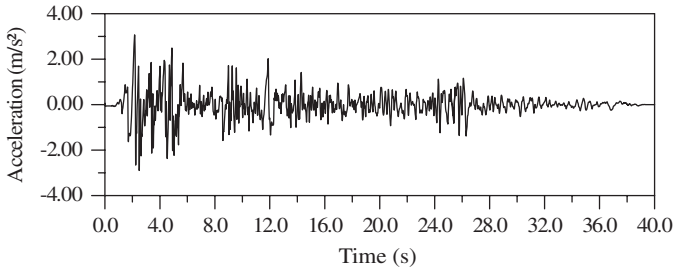

Fig. 4. The El-Centro N–S record of Imperial Valley earthquake, on May 18, 1940 (PEER: Pacific Earthquake Engineering Research Center, 2005).

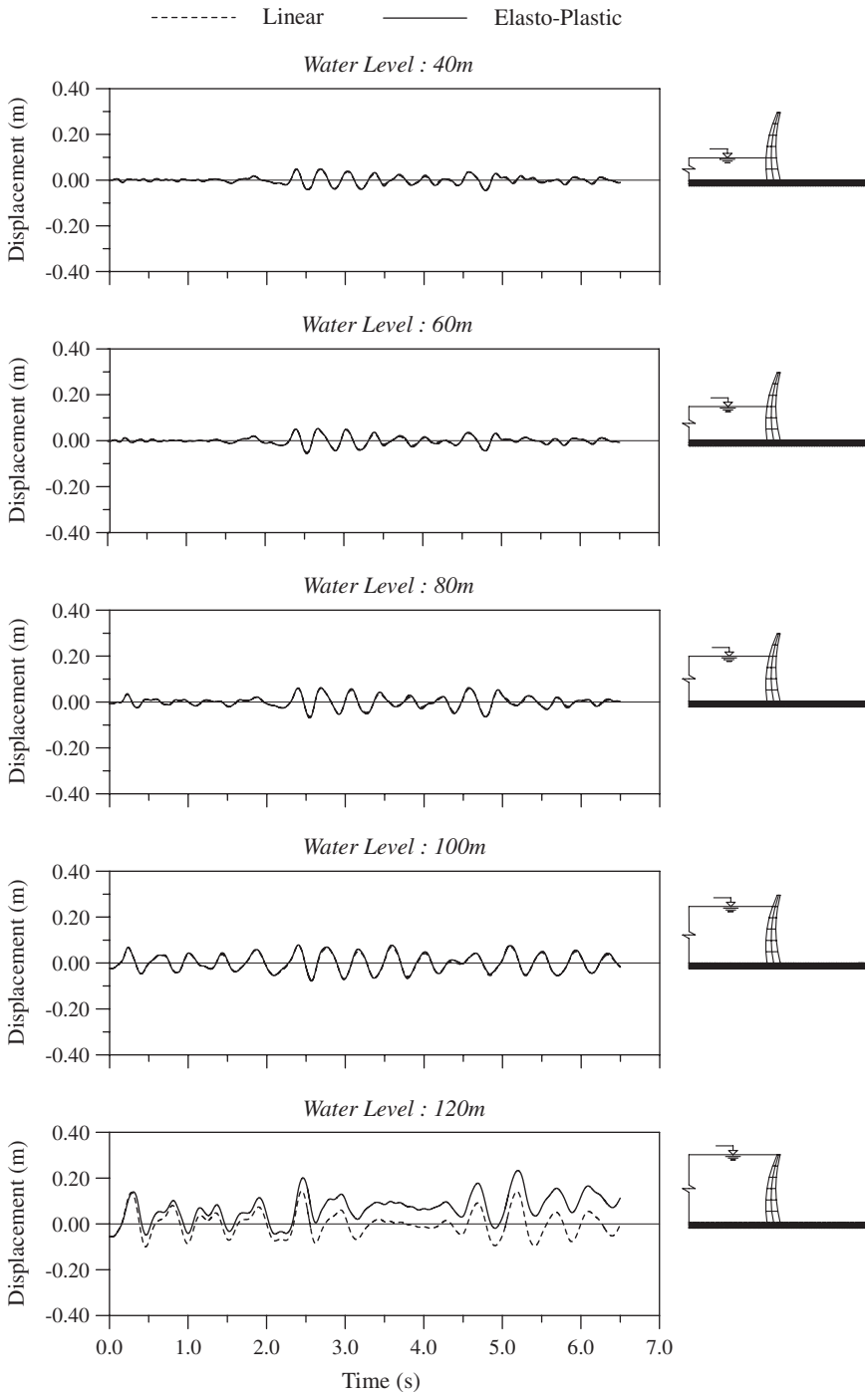

Fig. 5. The time histories of displacements at the crest of Type 5 arch dam *on rigid foundation rock* in the *y*-direction for reservoir water levels of 40, 60, 80, 100 and 120 m.

nonlinear analysis. The element A is on the upstream face of the dam. The section E–E is on the elements between 80 and 100 m from the base (Fig. 7). The stresses at section E–E of the arch dam are given in the *x*-direction since the arch action in the response of arch dams is generally pronounced. The stresses are calculated at the centre of the elements. Figs. 8 and 9 show the stresses on the upstream and downstream faces of the dam on rigid foundation rock,

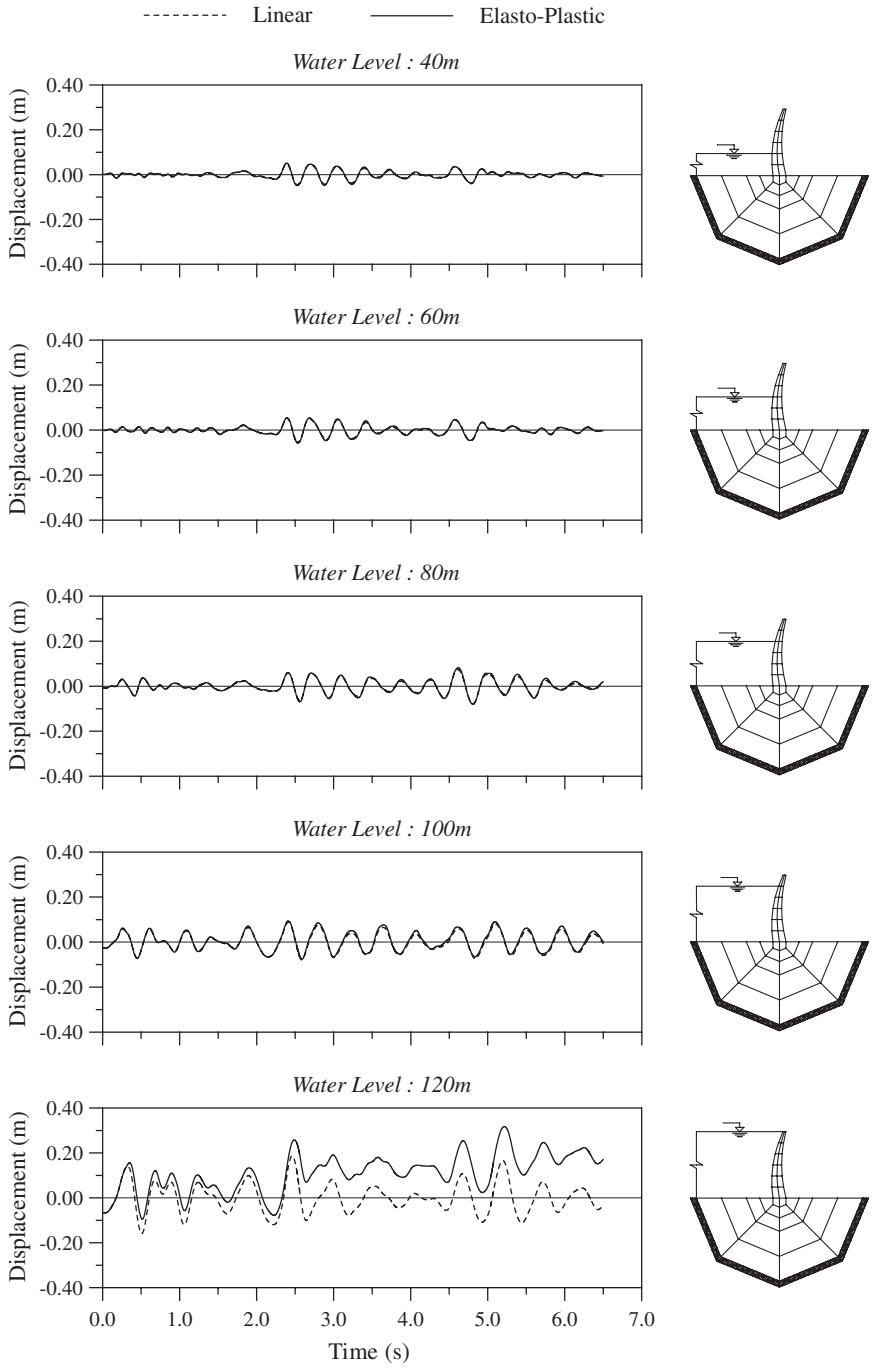

Fig. 6. The time histories of displacements at the crest of Type 5 arch dam *on flexible foundation rock* in the *y*-direction for reservoir water levels of 40, 60, 80, 100 and 120 m.

respectively. The corresponding stresses for the dam on flexible foundation rock are shown in Figs. 10 and 11. Here, the statement "the stresses on the upstream and downstream faces of the dam" means the stresses at the centre of the elements on upstream and downstream parts of dam. It can be seen from Figs. 10 and 11 that the stresses significantly increase after the water level in the reservoir reaches 60 m. There is an increase in the responses due to the increase in

Table 1
The absolute maximum crest displacements of Type 5 arch dam on rigid and flexible foundation rock for linear and elasto-plastic analyses

The absolute maximum crest displacements of Type 5 arch dam (m)				
Water level (m)	Linear analysis—foundation rock		Elasto-plastic analysis—foundation rock	
	Rigid	Flexible	Rigid	Flexible
40	0.046	0.049	0.049	0.052
60	0.052	0.055	0.055	0.057
80	0.064	0.077	0.069	0.082
100	0.075	0.088	0.079	0.094
120	0.145	0.187	0.233	0.317

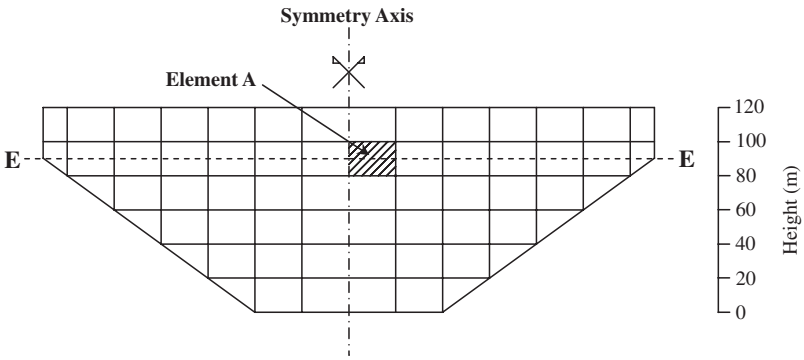

Fig. 7. The upstream view of Type 5 arch dam body.

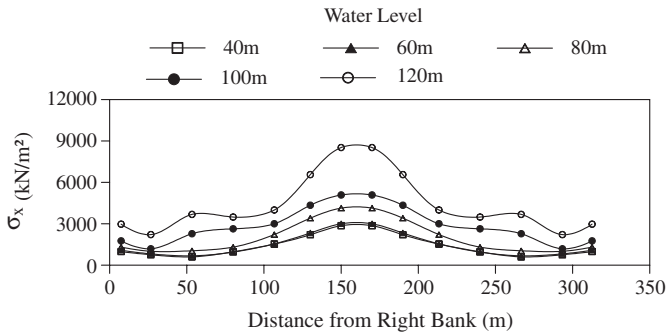

Fig. 8. Variation from right bank to left bank of maximum tensile stresses *on the upstream face* of Type 5 arch dam *on rigid foundation rock* for reservoir water levels of 40, 60, 80, 100 and 120 m in the *x*-direction at E–E section.

water level from 100 to 120 m. Due to the increase in the water levels, the stresses in the E–E section are significantly increased. In addition, decreasing the thickness of the dam across the crest caused an increase of the stresses.

A decrease is seen in the stresses at the elements in the middle of the dam along the section E–E for the water levels 80 and 120 m in Fig. 9 and for a water level 120 m in Fig. 11. On the other hand, an increase of the stresses occurs at the same elements for other water levels. It is thought that this situation occurs due to the dam geometry since arch dams are doubly curved and slender structures.

The time-histories of the yield function *f* at element A (Fig. 7) in the dam body are given in Figs. 12 and 13. As seen from Fig. 12, the element on the upstream face of the arch dam on rigid foundation rock for reservoir water levels 40,

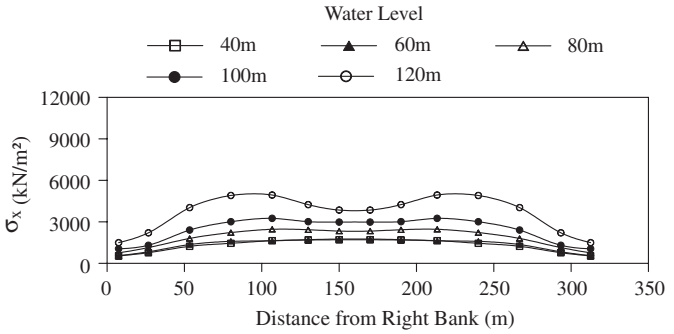

Fig. 9. Variation from right bank to left bank of maximum tensile stresses *on the downstream face* of Type 5 arch dam *on rigid foundation rock* for reservoir water level 40, 60, 80, 100 and 120 m in the *x*-direction at E–E section.

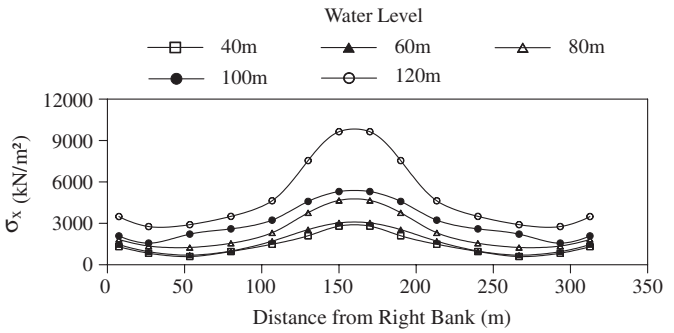

Fig. 10. Variation from right bank to left bank of maximum tensile stresses *on the upstream face* of Type 5 arch dam *on flexible foundation rock* for reservoir water level 40, 60, 80, 100 and 120 m in the *x*-direction at E–E section.

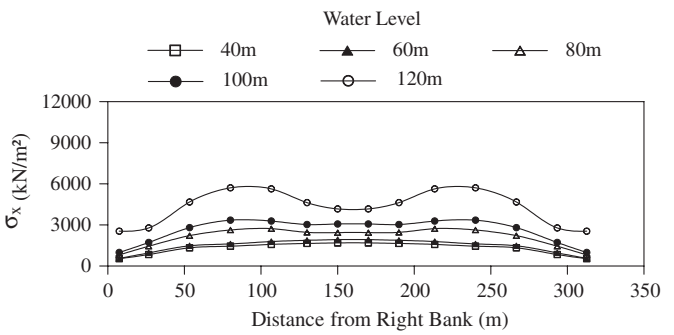

Fig. 11. Variation from right bank to left bank of maximum tensile stresses *on the downstream face* of Type 5 arch dam *on flexible foundation rock* for reservoir water level 40, 60, 80, 100 and 120 m in the *x*-direction at E–E section.

60, 80 and 100 m represents elastic behaviour since all values of the yield function are smaller than zero. As known, the values below zero of the yield function indicate that the element is in elastic state. Although the tensile stresses in the element increase due to the hydrodynamic effects, this represents elastic behaviour. However, plastic deformations occurred at the element due to the large tensile stresses for the water level of 120 m.

Fig. 13 presents the time-histories of the yield functions at element A on the upstream face of the arch dam on flexible foundation rock for reservoir water levels at 40, 60, 80, 100 and 120 m. After the water level reaches 60 m, plastic deformations occur at the element. As water level in the reservoir increases, the value of the yield function becomes zero many times. It is seen from the results that the water level in the reservoir considerably affects the elasto-plastic response of the arch dam.

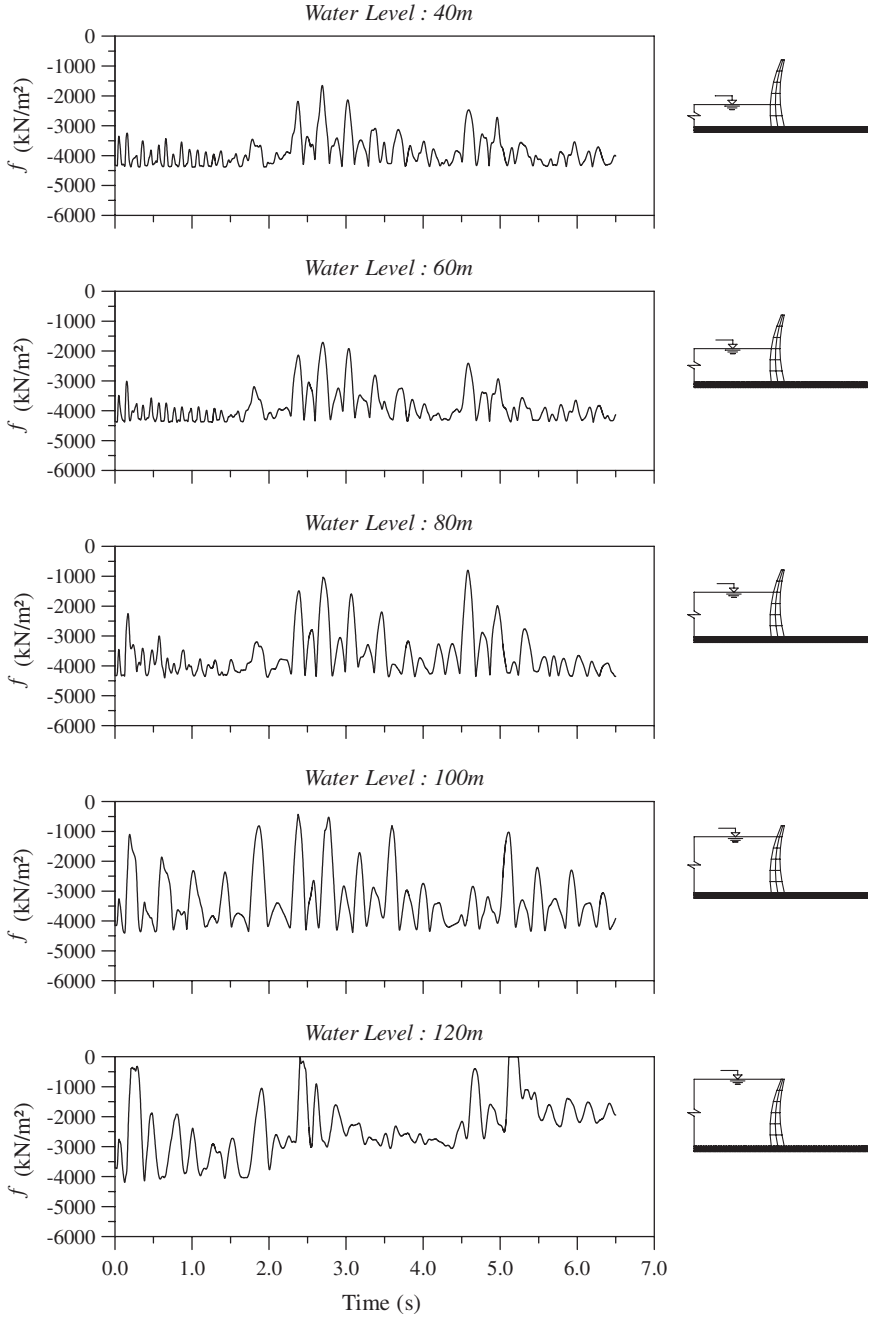

Fig. 12. Time histories of yield functions at element A *on the upstream face* of Type 5 arch dam *on rigid foundation rock* for reservoir water level 40, 60, 80, 100 and 120 m.

5. Conclusions

In this study, reservoir water level effects on the nonlinear dynamic responses of an arch dam are investigated by a Lagrangian approach in which a step-by-step integration technique is employed. The stress–strain behaviour of the dam concrete is idealized using the three-dimensional Drucker–Prager model based on the associated flow rule assumption. Water in reservoir is represented by eight-noded Lagrangian fluid finite elements. The results obtained from nonlinear analyses of a Type 5 arch dam on rigid and flexible foundation rock lead to the following conclusions.

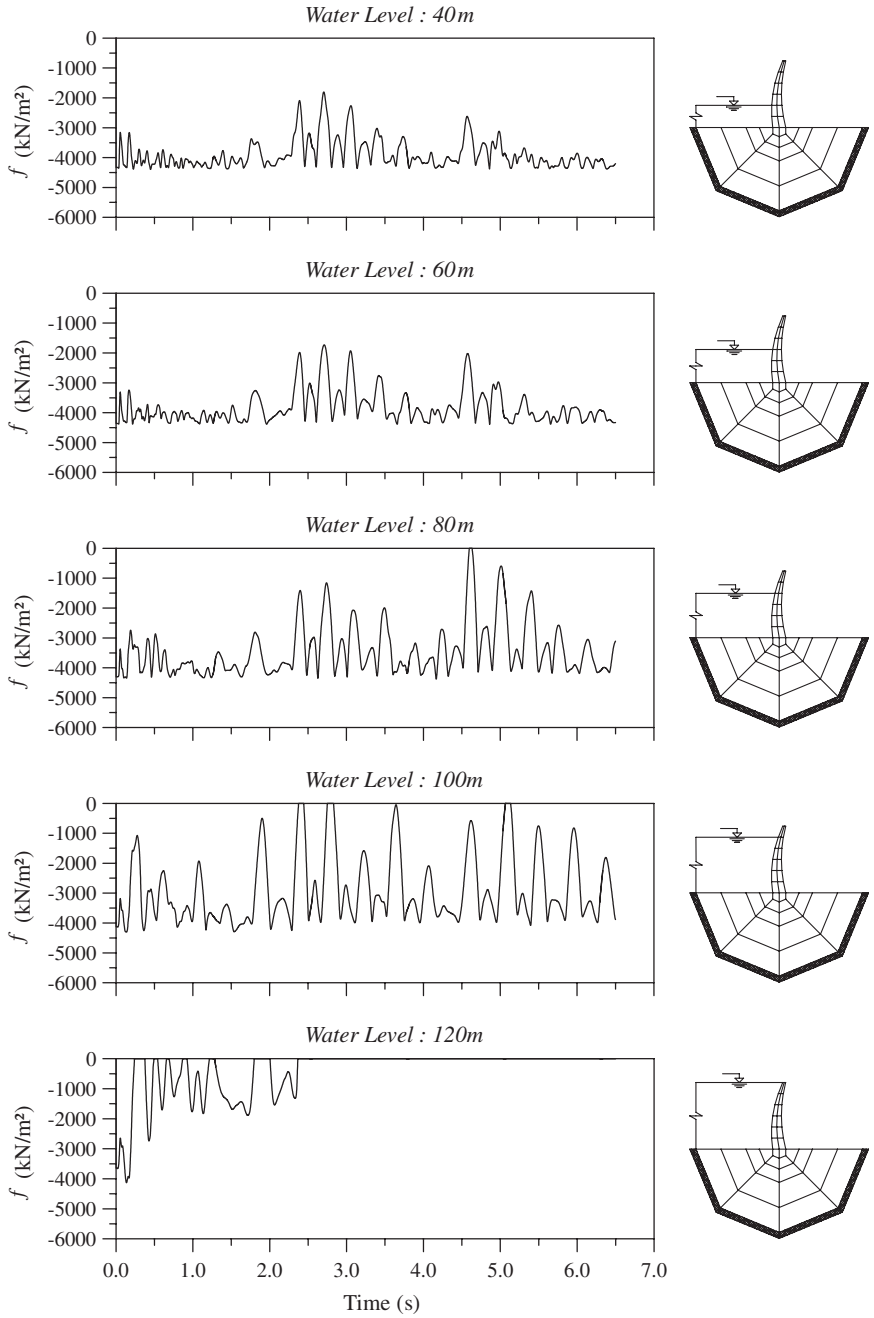

Fig. 13. Time histories of yield functions at element A *on the upstream face* of Type 5 arch dam *on flexible foundation rock* for reservoir water level 40, 60, 80, 100 and 120 m.

The results obtained from the elasto-plastic analysis of the arch dam shows a drift in the crest displacements. After a certain water level is reached, the crest displacements of the dam and the arch stresses on the dam body increase significantly. As can be seen from the results presented, this critical water level is 100 m for the dam on rigid foundation rock, and 60 m for the dam on flexible foundation rock.

The maximum tensile stresses in the dam body are considerably affected by increasing the water level in both linear and elasto-plastic analyses of the arch dam. It has been seen from the time histories of the yield functions of a selected

element near the crest in the dam body that element behaviour shows a plastic state after the water level reaches 100 m for rigid and 60 m for flexible foundation rock.

In the light of the conclusions, it is apparent that reservoir water level effects must be considered in the elasto-plastic analysis of arch dams to earthquake ground motion. In addition, in the linear analysis of a dam, overstressing problems in tensile and compressive stresses are encountered. The elasto-plastic model given in this study can overcome the problem and predict realistic distribution and levels of stresses in the dam body. It is thought that the elasto-plastic analyses of arch dams are very important for the determination of the plastic regions in the dam body.

Since the dynamic response of arch dams to earthquake loading is affected by several factors, including intensity and characteristics of the earthquakes, interaction of the dam with the foundation rock and reservoir water, computer modelling and material properties used in the analysis, the completed responses of Type 5 arch dam subjected to El-Centro earthquake ground motion should not be generalized to usual arch dams. Whereas the detailed observations may be dependent on the specific problem, the broad conclusions should apply to many cases.

References

Akkaş, N., Akay, H.U., Yılmaz, Ç., 1979. Applicability of general-purpose finite element programs in solid–fluid interaction problems. Computers and Structures 10, 773–783.

Akkose, M., 2004. Materially linear and nonlinear dynamic analyses of arch dam–water–foundation systems by Lagrangian approach (in Turkish). Ph.D. Thesis, Karadeniz Technical University, Trabzon, Turkey.

Bathe, K.J., 1996. Finite Element Procedures in Engineering Analysis. Prentice-Hall, Englewood Cliffs, NJ.

Bathe, K.J., Wilson, E.L., Iding, R., 1974. NONSAP: A Structural Analysis Program for Static and Dynamic Response of Nonlinear Systems. Structural Engineering and Structural Mechanics, Department of Civil Engineering, Report No. UC SESM 74-3, University of California, Berkeley, CA.

Calayır, Y., 1994. Dynamic analysis of concrete gravity dams using the Eulerian and Lagrangian approaches (in Turkish). Ph.D. Thesis, Karadeniz Technical University, Trabzon, Turkey.

Calayır, Y., Dumanoğlu, A.A., 1993. Static and dynamic analysis of fluid and fluid–structure systems by the Lagrangian method. Computers and Structures 49 (4), 625–632.

Calayır, Y., Dumanoğlu, A.A., Bayraktar, A., 1996. Earthquake analysis of gravity dam–reservoir systems using the Eulerian and Lagrangian approaches. Computers and Structures 59 (5), 877–890.

Chen, W.F., Mizuno, E., 1990. Nonlinear Analysis in Soil Mechanics. Elsevier Science Publishers B.V., Amsterdam, Netherlands.

Clough, R.W., Penzien, J., 1993. Dynamics of Structures, second ed. McGraw-Hill Book Company, Singapore.

Drucker, D.C., Prager, W., 1952. Soil mechanics and plastic analysis on limit design. Quarterly Journal of Applied Mathematics 10, 157–165.

Espandar, R., Lotfi, V., 2003. Comparison of non-orthogonal smeared crack and plasticity models for dynamic analysis of concrete arch dams. Computers and Structures 81, 1461–1474.

Fok, K.L., Chopra, A.K., 1986a. Hydrodynamic and foundation flexibility effects in earthquake response of arch dams. Journal of Structural Engineering 112 (8), 1810–1828.

Fok, K.L., Chopra, A.K., 1986b. Earthquake analysis of arch dams including dam–water interaction, reservoir boundary absorption and foundation flexibility. Earthquake Engineering and Structural Dynamics 14, 155–184.

Greeves, E.J., 1991. The modelling and analysis of linear and nonlinear fluid-structure systems with particular reference to concrete dams. Ph.D. Thesis, Department of Civil Engineering, University of Bristol, UK

Hall, J.F., 1998. Efficient nonlinear seismic analysis of arch dams. Earthquake Engineering and Structural Dynamics 27, 1425–1444.

Hamdan, F.H., 1999. Near-field fluid–structure interaction using Lagrangian fluid finite elements. Computers and Structures 71, 123–141.

ICE, 1968. Arch dams: a review of British research and development. In: Proceedings of the Symposium held at the Institution of Civil Engineers, 20–21 March, London, England.

Kuo, J.S.H., 1982. Joint opening nonlinear mechanism: interface smeared crack model. Earthquake Engineering Research Center, Report No. UCB/EERC-82/10, University of California, Berkeley, CA, USA.

Olson, L.G., Bathe, K.J., 1983. A study of displacement-based fluid finite elements for calculating frequencies of fluid and fluid–structure systems. Nuclear Engineering and Design 76, 137–151.

PEER: Pacific Earthquake Engineering Research Center, 2005. 〈http://peer.berkeley.edu/smcat/data〉.

Perumalswami, P.R., Kar, L., 1973. Earthquake behavior of arch dams-reservoir systems. In: Fifth World Conference on Earthquake Engineering, Rome, Italy.

Proulx, J., Paultre, P., Rheault, J., Robert, Y., 2001. An experimental investigation of water level effects on the dynamic behaviour of a large arch dam. Earthquake Engineering and Structural Dynamics 30, 1147–1166.

Tan, H., Chopra, A.K., 1995a. Earthquake analysis of arch dams including dam–water–foundation rock interaction. Earthquake Engineering and Structural Dynamics 24, 1453–1474.

Tan, H., Chopra, A.K., 1995b. Dam–foundation rock interaction effects in frequency-response functions of arch dams. Earthquake Engineering and Structural Dynamics 24, 1475–1489.

Valliappan, S., Yazdchi, M., Khalili, N., 1999. Seismic analysis of arch dams-a continuum damage mechanics approach. International Journal for Numerical Methods in Engineering 45, 1695–1724.

Wilson, E.L., Khalvati, M., 1983. Finite elements for the dynamic analysis of fluid–solid systems. International Journal for Numerical Methods in Engineering 19, 1657–1668.

Zienkiewicz, O.C., Bettes, P., 1978. Fluid–structure dynamic interaction and wave forces. An introduction to numerical treatment. International Journal for Numerical Methods in Engineering 13, 1–16.

Zienkiewicz, O.C., Taylor, R.L., 1989. The Finite Element Method, vol. 1. McGraw-Hill, London.